Available online at www.sciencedirect.com
SCIENCE DIRECT®
Journal of Molecular Catalysis A: Chemical 229 (2005) 95–105
JOURNAL OF MOLECULAR CATALYSIS A: CHEMICAL
www.elsevier.com/locate/molcata

Photocatalytic degradation of pesticide pyridaben on TiO_2 particles

Xinle Zhu[a,d,*], Chunwei Yuan[a,d], Yanchu Bao[b], Jihong Yang[b], Yizu Wu[c]

[a] *The Laboratory of Nano-materials and Photocatalysis, Department of Biomedical Engineering, Southeast University, No. 2, Sipailou, Nanjing 210096, PR China*
[b] *Center of Materials Analysis, Nanjing University, Nanjing 210093, PR China*
[c] *College of Chemistry and Chemical Engineering, Nanjing Technology University, Nanjing 210009, PR China*
[d] *The Key Laboratory of Molecular and Biomolecular Electronics, Department of Biomedical Engineering, Southeast University, Nanjing 210096, PR China*

Received 3 July 2004; received in revised form 12 November 2004; accepted 12 November 2004
Available online 24 December 2004

Abstract

The TiO_2 photoassisted degradation of pesticide pyridaben has been examined in acetonitrile/water suspensions under UV light irradiation mainly at wavelength longer than 360 nm. To distinguish from the accompanying photolytic phenomenon, the kinetics of direct photolytic and photocatalytic degradation of pyridaben in TiO_2 suspensions were studied by two different UV wavelength irradiations ($\lambda \geq 300$ nm and $\lambda \geq 360$ nm). The results manifested that the photolysis or photocatalysis of pyridaben followed pseudo-first-order kinetics, the direct photolysis was dominant at $\lambda \geq 300$ nm, and the higher photocatalytic efficiency was obtained at $\lambda \geq 360$ nm. The photocatalytic degradation kinetics were studied under different conditions such as water content, pH, catalyst concentration as well as radiant flux, and the degradation rates were found to be strongly influenced by these parameters. A qualitative study of the degradation products generated during the process was performed by GC–MS. Up to fifteen compounds were detected as degradation intermediates, many of which were identical with those detected previously at $\lambda \geq 300$ nm. We also analyzed the evolution of the degradation products semiquantitatively by plotting areas of the corresponding GC peaks as functions of irradiation time. Moreover, a complementary study using molecular model calculation was performed to forecast pyridaben's adsorption point on TiO_2 particles and its weak position of molecular cleavage. On the basis of the analytical and kinetic results, a degradation mechanism was proposed. This work is significant to understand the photochemistry of pesticide pyridaben in the environmental treatment.

Keywords: Pyridaben; Photocatalysis; Photolysis; Kinetics; Mechanisms; TiO_2

1. Introduction

In recent two decades, heterogeneous photocatalysis has emerged as an efficient technology to purify air and water [1–4]. This technique is based upon the use of UV irradiated semiconductors, generally titanium dioxide, to destroy various organic pollutants. Through a large number of reported studies the basic mechanism of photocatalysis has been well established, i.e., organic molecules react with the light-induced holes or with the radicals coming from water or from the adsorbed oxygen to be oxidized to inorganic compounds as CO_2 and H_2O [1–6].

Among the organic compounds of insecticide concern, pyridaben is used as an effective substitute for some traditional pesticides for the control of a range of agronomic pests, particularly lepidoptera, in cereals, fruits, vegetables, and other crops [7–9], (Fig. 1). Due to its high recalcitrance, there presents a remediation challenge in wastewaters originated from the pesticide industry. Therefore, we selected it as the model compound to investigate the behavior of photocatalytic degradation.

In our previous research, the degradation of pyridaben under UV lamp at $\lambda \geq 300$ nm using suspended TiO_2 has been

* Corresponding author. Tel.: +86 25 83794310; fax: +86 25 83793091.
E-mail address: zhuxinle@seu.edu.cn (X. Zhu).

1381-1169/$ – see front matter © 2004 Elsevier B.V. All rights reserved.
doi:10.1016/j.molcata.2004.11.010

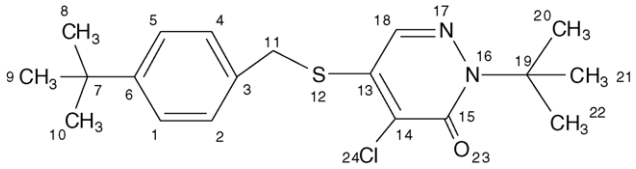

Fig. 1. Molecular structure of pyridaben.

reported, with main attention devoted to the identification of the intermediates and reaction pathways [10]. In the present, we performed the investigation at $\lambda \geq 360$ nm wavelength irradiation. Attention was focused on the determination of optimal operation parameters such as solvent effect, pH, catalyst loading and flux radiant. Another objective was to demonstrate that the truly photocatalytic behavior depended on the irradiation wavelength, which was derived by comparing the photodecay behavior of pyridaben at $\lambda \geq 300$ nm with that at $\lambda \geq 360$ nm. On mechanism study, the intermediate identification as well as the formation and the fate of aromatic products were investigated by GC–MS. The characteristic bell-shaped behavior of intermediates was depicted as functions of the corresponding peak area as irradiation time, upon which the photodegradation mechanism of pyridaben has been further verified. The measurement of the degradation processes will permit us to bring solutions to remediate water pollution of pesticide industries efficiently.

2. Experiment

2.1. Materials

Pyridaben was obtained from Jiangsu Red Sun Co. Ltd., and used with purification to 99.92%. The semiconductor employed as photocatalyst was commercial titanium dioxide (Degussa P25), with a crystallographic mode of 80% anatase and 20% rutile according to the manufacturer's specifications. HPLC-grade acetonitrile and methanol were purchased from Tedia Company Inc. Water used was Ultra-Pure water from Jiangsu Bote purified Water Co. Ltd. All other reagents utilized were of analytical purity.

2.2. Photoreactor and light source

The UV-light source was a 350 W medium-pressure mercury lamp (Institute of Electric Light Source, Beijing) with main emission wavelength at 365 nm, as shown in Fig. 2, which was positioned inside a cylindrical quartz vessel that was surrounded by a circulating water jacket to cool the lamp. The optical filters were placed outside the quartz jacket to ensure complete removal of radiation below 360 nm or 300 nm, respectively, the corresponding spectral distributions being displayed in Fig. 2. The intensity of the irradiation at $\lambda \geq 300$ nm or $\lambda \geq 360$ nm was regulated to 7.8 mW/cm^2. The

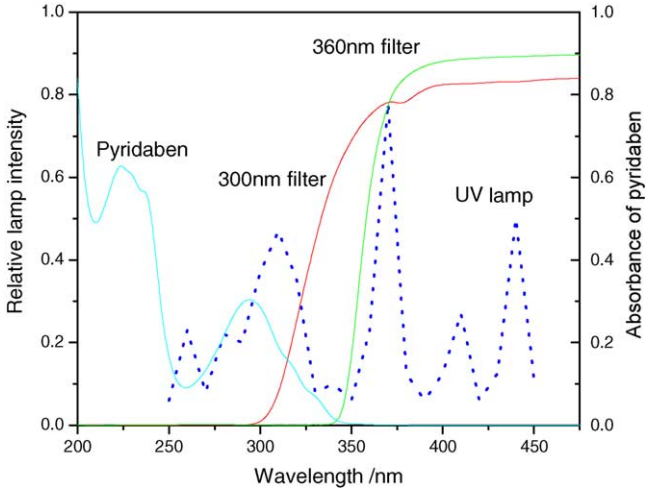

Fig. 2. The emission spectrum of UV-lamp and those through different filters as well as the UV–vis spectrum of pyridaben.

reactor was wrapped with aluminum foil to shield against other laboratory light sources. All experiments were performed with TiO_2 powder (2.5 g/L), kept for 60 min in the dark to equilibrate and studied at natural pH (6.0) unless otherwise stated.

2.3. General procedure and analysis

In kinetic experiments, a known amount of pyridaben was dissolved in 20 ml solvent (CH_3CN/H_2O = 80/20) in the photoreactor, resulting in a solution with concentration of 40 ppm (C_0 = 0.1097 mM). Samples were taken at regular irradiation time intervals, centrifuged and filtered with 0.22 μm Millipore filter to remove TiO_2 particle. The amounts of pyridaben in the test solutions were evaluated with HPLC analysis (996 photodiode array detector and a waters 510 pump). The eluent was a methanol–water mixture (85/15, v/v).

In intermediate identification and evolution processes, the solution with concentration of 120 ppm (0.3292 mM) was stopped at the desired time of irradiation, and then the whole volume of the suspension was collected and filtered to allow for qualitative and semiquantitative determination. Preparation of samples and methods employed for GC–MS measurements has been described in detail elsewhere [10].

2.4. Computer simulation

The optimal geometry conformation and the lowest energy of pyridaben molecule were obtained at PM3 level. By calculating the values of the point charge and bond length we predicted the adsorption sites on TiO_2 particles and the weak position of the molecule in the initial reaction process. Calculations were carried out using Hyperchem, version 5.0.

Table 1
Kinetic parameters of photodecay processes in different wavelengths

	Photolysis ≥ 300 nm	Photocatalysis ≥ 300 nm	Photolysis ≥ 360 nm	Photocatalysis ≥ 360 nm
k (min^{-1})	0.0759	0.0673	0.0034	0.0343
$t_{1/2}$ (min)	9.13	10.30	203.82	20.20
R (%)	98.75	99.43	99.29	97.81

3. Results and discussion

Identification of the optimal conditions for pyridaben, such as irradiation wavelengths, catalyst concentration, pH, solvent effect and light intensity, will be discussed as follows.

3.1. The effect of photolysis and photocatalysis

Since the photodegradation of pyridaben involves direct photolysis and photocatalysis, it is necessary to understand its decay behavior under corresponding conditions. Fig. 2 displays the emission spectrum of UV lamp and those through 300 nm and 360 nm optical filters as well as the UV absorption spectrum of pyridaben. We observed that pyridaben molecule presents a measurable absorption tailing up to 300 nm, whereas at $\lambda \geq 360$ nm is far below the limit, therefore at $\lambda \geq 300$ nm wavelength irradiation, the photolytic degradation reaction should not be neglected.

To verify this assumption, experiments were made in the absence (neat photolytic regime) and presence of TiO_2 with two different kinds of optical filters. As indicated in Fig. 3, the total disappearance of pyridaben in photocatalysis was achieved within 60 min and 140 min by $\lambda \geq 300$ nm and $\lambda \geq 360$ nm irradiation, respectively. The pseudo-first-order kinetics linear transforms of photodecay pyridaben are given in Fig. 4, which are confirmed by the linear behavior of $\ln(C_0/C)$ as a function of irradiation time. The kinetic parameters are listed in Table 1.

By $\lambda \geq 300$ nm irradiation, the reaction rate of photolysis is faster than that of photocatalysis, which suggests that the photodecay of pyridaben be dominated by direct photolysis. Pyridaben has a feature of absorption around 300 nm wavelength; therefore, it would be excited by absorbing corresponding UV light with sufficient energy, resulting in higher photolytic rate. Nevertheless, the presence of catalyst particles in the suspension reduces the absorption of UV photon ($300\ nm < \lambda < 350$ nm) by pyridaben; consequently, the reaction rate decreases. Hu et al. have studied the TiO_2-mediated photocatalytic oxidation of phenol, indicated that UV light in the range of $200\ nm < \lambda < 300$ nm played a somewhat detrimental role in the photodegradation of phenol [11]. Similar reaction have been obtained by Wong and Chun that the photolysis were dominant at 254 nm in degradation of alachlor even if TiO_2 was present in the solution [12].

Illuminating pyridaben solution with UV light at $\lambda \geq 360$ nm, in the presence of TiO_2, results in the decomposition of the substrate about 10 times faster than that in the absence of catalyst, indicating that the application of a TiO_2-mediated photocatalytic nature is confirmed. As shown in Fig. 2, there is almost no absorption of pyridaben in the range of wavelength ≥360 nm, so that this illumination is capable of photoexciting TiO_2 but not significantly absorbed by pyridaben. In other words, there occurs the photocatalysis,

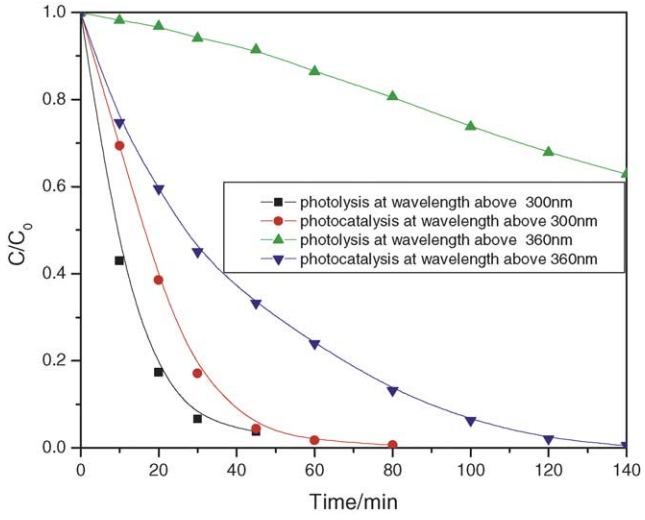

Fig. 3. Plots of the normalized concentration as of irradiation time for the photolysis and photocatalysis of pyridaben at $\lambda \geq 360$ nm or $\lambda \geq 300$ nm irradiation.

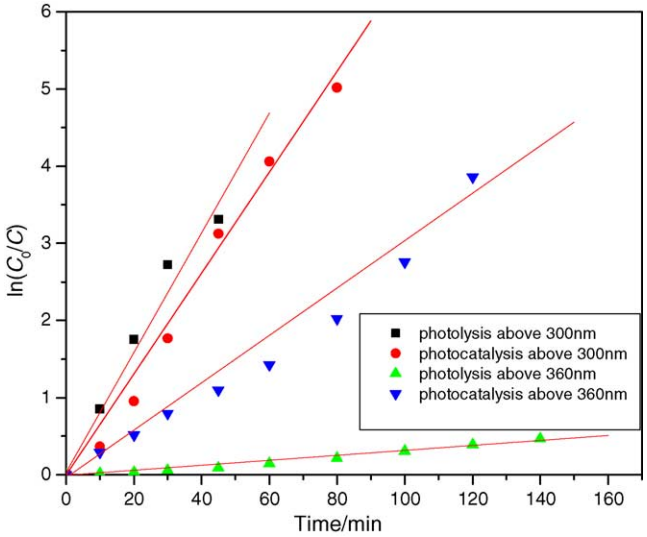

Fig. 4. Pseudo-first-order linear transforms of disappearance of pyridaben by the photolysis and photocatalysis at $\lambda \geq 300$ nm or $\lambda \geq 360$ nm irradiation.

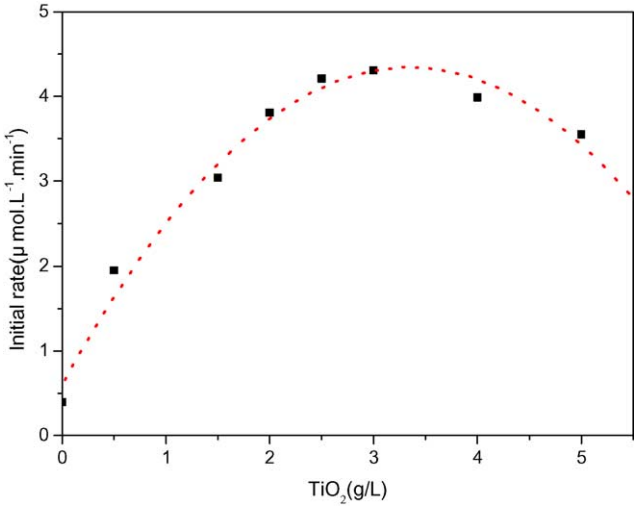

Fig. 5. Influence of titania concentration on the initial reaction rate of pyridaben.

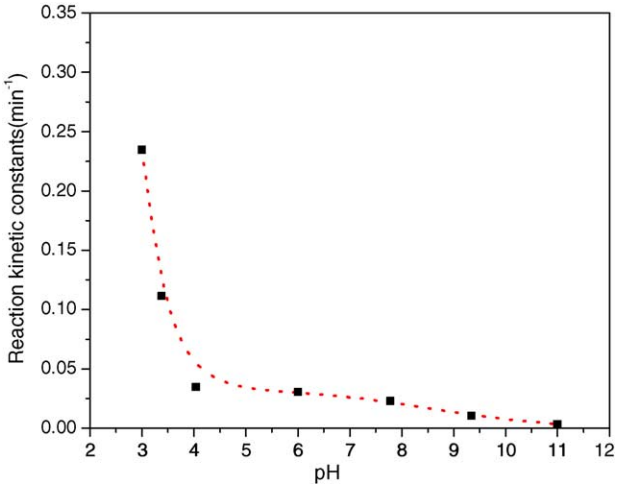

Fig. 6. Influence of pH on the kinetic rate constant of pyridaben photocatalytic disappearance.

but the photolytic reaction would not come into play. Since irradiation wavelength at $\lambda \geq 360$ nm is among the best for pyridaben photocatalytic degradation, in what follows, it will be used systematically.

3.2. Determination of the optimum concentration of titania

Experiments were carried out with TiO_2 concentrations ranging from 0 to 5 g/L to determine the optimum catalyst loading. Fig. 5 displays the variation of the initial rates of degradation versus photocatalyst loading for experiments with an initial pyridaben concentration of 1.0974×10^{-4} mol/L.

As expected, at low photocatalyst loadings, the curve of removal of organic compounds exhibits a linear increasing until 2.5 g/L TiO_2 is used, which indicates that the reaction rate is proportional to the total surface exposed. As the concentration of TiO_2 increases, the plot shows a maximum in initial reaction rate around from 2.5 g/L to 3.5 g/L TiO_2, suggesting a progressive saturation of the photonic absorption for a given radiant flux. However, as the TiO_2 concentration increases continuously the reaction rate decreases. This is due to the shielding of incident light by TiO_2 particles, in other words, increased turbidity of the suspension reduces the light transmission. Furthermore, increase of light scattering would also reduce the photonic flux within the irradiated solution [1,3,13]. Evidently, the maximum photoactivity from the available light is achieved when the concentration of catalyst attains to 2.5 g/L, which will be used for the rest of this study.

3.3. Effect of pH

The real effluent stuff of pesticide can be discharged at different pH, therefore the effect of pH on the rate of photocatalytic degradation of pyridaben was studied in the range between pH 3 and pH 11, altered by HCl or NaOH solutions. The kinetic rate constant for the degradation of pyridaben (0.1097 mM) as a function of reaction pH is shown in Fig. 6. As reported, the pH of the suspension appears to have little effect on the rate of disappearance of pyridaben between pH 4.5 and pH 6.5 and gradually decreases upon increasing the pH from pH 7.0 to pH 11.0. The most outstanding is that the marked increase in the rate occurs when pH is decreased below 4.0. Control experiments demonstrated that the hydrolysis or photolysis of pyridaben was negligible with respect to the photocatalytic decomposition at the initial pH 3.0, evidencing that a true photocatalytic process is operable.

The zero point of charge (zpc) of semiconductor particles is defined as the pH at which the concentrations of protonated and deprotonated group are equal, i.e. pH zpc = $1/2(pK_1 + pK_2)$. The pH zpc of TiO_2 is 6.25, so its surface is predominately positively charged below pH zpc, i.e. $Ti{-}OH + H^+ \rightleftharpoons TiOH_2{}^+$ and negatively charged above, i.e. $Ti{-}OH + OH^- \rightleftharpoons TiO^- + H_2O$. Therefore, pH value will have a significant effect on the adsorption/desorption properties at the catalyst's surface [1,14,15].

At natural pH value (pH 6.0), TiO_2 surface carries a weakly positive charge, while pyridaben is primarily neutrally charged, which could facilitate the adsorption of the substrate and promote better photocatalytic degradation. In order to further predict some details of the adsorption mode of pyridaben on the TiO_2 surface, point charges of all individual atoms in pyridaben molecule were calculated by means of PM3 method, which has been reported by Guillard et al. [16], and Horikoshi et al. [17,18]. The results are summarized in Table 3. Information indicates that a strong negative charge is located on the oxygen atom of $-O{=}C-$ group, therefore under the natural condition (pH 6.0), the photocatalyst surface is positively charged and attractive force between the $Ti{-}(OH_2)^+$ surface groups and the pyridaben molecules, as presented in Fig. 12, is operable. By contrast, the adsorption is inhibited by high pH values.

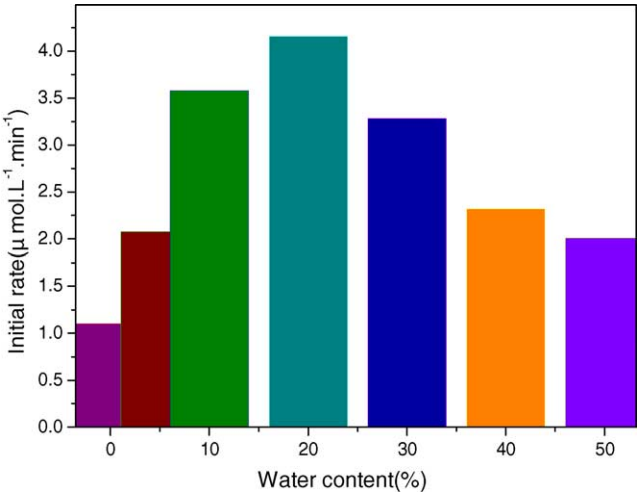

Fig. 7. Effect of water content on the initial reaction rates of photocatalytic degradation of pyridaben.

Under pH 3.0 to pH 4.0 the substrate molecule could be in disfavor of adsorption on TiO_2 surface in positive ionic form, which seems to conflict with the experimental results. However, as suggested by several authors [19–21], the pH and the anions of the solution would also affect the formation of hydroxyl free radicals, the agglomerated effective particle size, and the band edge positions of TiO_2. These factors would have an effect upon the photocatalytic reaction.

3.4. The solvent effect

The model compound is poorly soluble in water and its direct detection in aqueous solution is limited with our Waters PDA system also. Therefore, we conducted the photocatalytic oxidation using acetonitrile as a co-solvent system.

We have studied the reactivities of pyridaben in acetonitrile solutions containing 0%, 5%, 10%, 20%, 30%, 40% and 50% of redistilled water, and calculated the initial reaction rate using the equation, $r_0 = C_0 \times k$. Fig. 7 shows the initial reaction rates of pyridaben disappearance in different water content solvents. The initial reaction rates follow the sequence: acetonitrile/H_2O (80/20) > (90/10) > (70/30) > (60/40) > (95/5) > (50/50) > (100/0). This order may be strongly related to hydroxyl radicals generated and the solubility of pyridaben in different cases. In general, more $^{\bullet}$OH groups may be photo-produced as the ratio of water increases if the water content is very limited. We deduce that the content of $^{\bullet}$OH increases in the order of 0%, 5%, 10% and 20% water content. Therefore, sufficient water was needed in organic solvent to generate hydroxyl radicals to participate in the photocatalytic reaction.

However, continuously increasing H_2O content in acetonitrile to a certain extent could decrease the reactivity. The initial rate decreases in the presence of water, going from 4.158×10^{-6} mol/L min^{-1} in acetonitrile/H_2O (80/20) to 3.285×10^{-6} mol/L min^{-1} in acetonitrile solution containing 30% water. When more water is present, for example 40% and 50% content (the latter attains the saturation solubility of pyridaben), the initial rate values become relatively low. Because the solubility of pyridaben decreases with increasing water, we deduce that the overdose water in the solution would reduce the possibility of contact of substrate with TiO_2 surface [22,23]. In addition, the solubility of oxygen in acetonitrile solution decreases with increasing water content. Matsuzawa et al. obtained a similar result in case of the study on photocatalysis of sulfur compounds [24]. Of course, the above results need to be further verified by electron spin resonance (ESR).

For application of this work, studies on the photocatalytic degradation of trace pyridaben in aqueous solution are in progress by using solid-phase extraction (SPE) techniques in our laboratory. The result will be reported and be contributive to the treatment of polluted water in pesticide industries.

3.5. Effect of light intensity

Experiments have been made corresponding to radiant fluxes (φ) varying from 2.8 to 8.8 mW/cm^2 in the range of our UV lamp being regulated. As represented in Fig. 8, the photocatalytic efficiency increases as the radiant fluxes of the lamp is increased; in other words, the reaction rate is proportional to φ and the process works in a good photocatalytic regime. This finding indicates that the incident photons are efficiently converted into active species that act in the degradation mechanism. Thus, the higher intensities will produce the higher rates without losing efficiency, which has been observed by many research groups [3,25].

3.6. Identification of transient photoproducts

More investigations aiming at identification of all organic intermediates would be necessary before a detailed mechanistic scheme can be proposed for the oxidation of pyridaben by

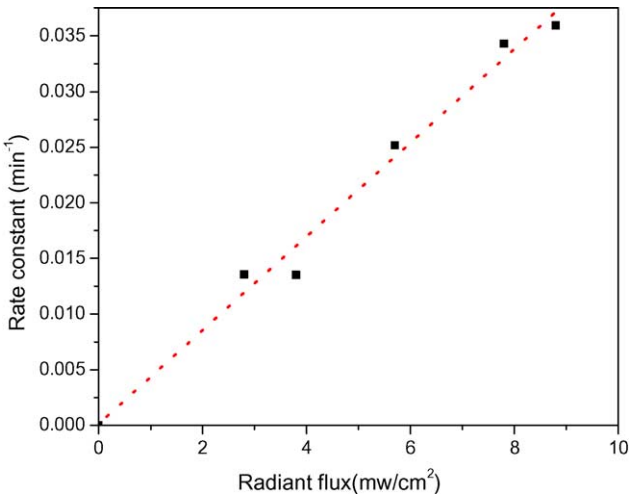

Fig. 8. Dependence of rate constant on light intensity.

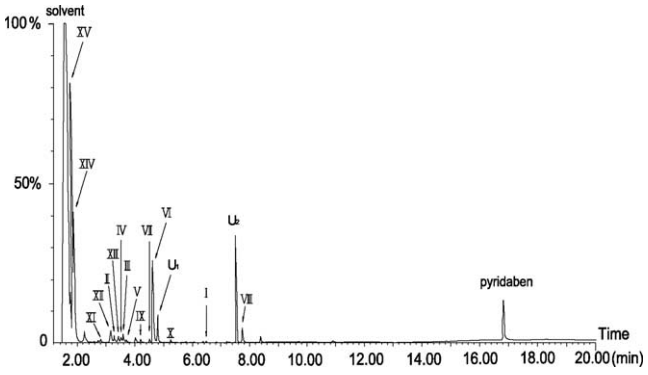

Fig. 9. Gas chromatogram of pyridaben and intermediates in photocatalysis for 340 min.

TiO_2 photocatalysis. Fig. 9 shows the total ion chromatogram obtained by GC–MS analysis of pyridaben suspension after irradiation for 340 min. Up to 15 compounds could be detected as possible degradation intermediates. Six of them were reported in the previous work (compound I to compound VI) [10]. Products (VIII, IX, X, XI, XII, XIII, XIV and XV were identified by comparing GC–MS spectra with those reported in the Nist and/or Willey library with a fit value higher than 90% in all cases. Aliphatic intermediates XIV and XV were presumed as the result of phenyl ring opening. Compounds found at t_R 4.80 min and 7.55 min were detected as unknowns U_1 and U_2, respectively, which were not identified but could be regarded as DPs (degradation products) because their concentration increased and decreased as a function of the reaction time. The mass spectrum of U_1 manifests the character of phenyl ring and that of U_2 shows common ions related with pyridazine compound.

The molecular ion and mass spectrometric fragmentation peaks along with their relative intensities for different products are given in Table 2.

The compound appears in t_R 4.5 min was deduced as VII. The molecular ion and mass spectrometric fragmentation peaks along with their relative intensities are given in Fig. 10 and the MS interpretation in Fig. 11. The molecular ion and basic peak of double signals 220/222 and 165/167 appear to be in a ratio of 3:1 due to the natural ratio of the isotopes of chloride 35/37. According to this, the product can be confirmed containing chloride. In addition, fragments at *m/z* 135 (M^+–C_4H_7–COH_2), 72 (M^+–C_4H_8–N_2–CO–HCl), 57 ($^+C_4H_9$), 56 (C_4H_8) are presented, which exhibit the identical loss with previously synthesized compound. Upon identified intermediates, a degradation pathway of photocatalysis of pyridaben has been proposed in Fig. 12.

Table 2
GC–MS–EI retention times (R_t) and spectrum characteristics of pyridaben and its major photoproducts

Insecticide photoproducts	R_t (min)	EI–MS spectrum ions (*m/z*) (% abundance)
Pyridaben	16.83	364(M^+) (5), 309 (20), 311 (4), 217 (3), 147 (100), 132 (5), 117 (6), 55 (6), 56 (17), 57 (3)
(VII) 2-*tert*-Butyl-4-chloro-6-mercapto-2,3-dihydropyridazin-3-ol	4.50	220(M^+) (2), 222(1), 164 (11), 166 (4), 165 (100), 167 (45), 135 (7), 136 (2), 107 (2), 55 (3), 56 (13), 57 (12)
(VIII) 2,5-di-*tert*-Butylaniline	7.75	205(50,M^+), 206 (5), 190 (100), 162 (4), 148 (30), 131 (26), 130 (3), 106 (40), 91 (5), 74 (2), 57 (5)
(IX) 1-*tert*-Butyl-4-ethoxybenzene	4.20	164(14,M^+), 165 (10), 149 (100), 150 (50), 135 (5), 121 (22), 91 (5), 65 (10)
(X) 2-*tert*-Butyl-4-methylphenol	5.25	164(22,M^+), 165 (2), 149 (100), 121 (67), 91 (3), 76 (5), 65 (22), 43 (8)
(XI) Terephthalaldehyde	2.83	134(100, M^+), 133 (95), 105 (55), 77 (35), 51 (20)
(XII) 4-Acetylbenzonitrile	3.18	145(15,M^+), 130 (100), 132 (22), 102 (25), 43 (5)
(XIII) 1-(3,4-Dimethylphenyl) ethanone	3.42	148(12,M^+), 149 (2), 133 (100), 105 (33), 77 (14)
(XIV) Succinonitrile	1.97	80(8,M^+), 79 (79), 53 (100), 52 (6), 40 (5)
(XV) Methylmalononitrile	1.88	80(11,M^+),79 (82), 77 (4), 53 (100), 52 (8), 51 (5), 40 (8)
(U_1)	4.80	202(3,M^+), 204 (1), 160 (73), 159 (18), 145 (13), 131 (100), 115 (31), 117 (17), 91 (58)
(U_2)	7.55	243(3,M^+), 245 (1), 191 (2), 190 (14), 188 (100), 187 (5), 130 (3), 57 (9), 56 (7), 55 (2)

Table 3
Point charge and bond length on atoms of pyridaben at the PM3 level

Atoms	Point charge	Bond	Bond length	Atoms	Point charge	Bond	Bond length
C^1	−0.108	C^1—C^2	1.1012	C^{13}	−0.162	S^{12}—C^{13}	1.7502
C^2	−0.075	C^2—C^3	1.3889	C^{14}	−0.235	C^{13}—C^{14}	1.3644
C^3	−0.098	C^3—C^4	1.3966	C^{15}	0.0276	C^{14}—C^{15}	1.4735
C^4	−0.0088	C^4—C^5	1.3878	N^{16}	0.063	C^{15}—N^{16}	1.4449
C^5	−0.0106	C^5—C^6	1.3968	N^{17}	−0.052	N^{16}—N^{17}	1.3568
C^6	−0.056	C^6—C^1	1.3964	C^{18}	−0.159	N^{17}—C^{18}	1.3121
C^7	0.003	C^6—C^7	1.516	C^{19}	0.038	C^{18}—C^{13}	1.4416
C^8	−0.119	C^7—C^8	1.5279	C^{20}	−0.122	C^{16}—C^{19}	1.5335
C^9	−0.119	C^7—C^9	1.5309	C^{21}	−0.144	C^{19}—C^{20}	1.5357
C^{10}	−0.0113	C^7—C^{10}	1.5296	C^{22}	−0.145	C^{19}—C^{21}	1.5326
C^{11}	−0.116	C^3—C^{11}	1.4867	O^{23}	−0.357	C^{19}—C^{22}	1.5328
S^{12}	0.115	C^{11}—S^{12}	1.8325	Cl^{24}	0.177	C^{15}—O^{23}	1.2226
						C^{15}—Cl^{24}	1.6661

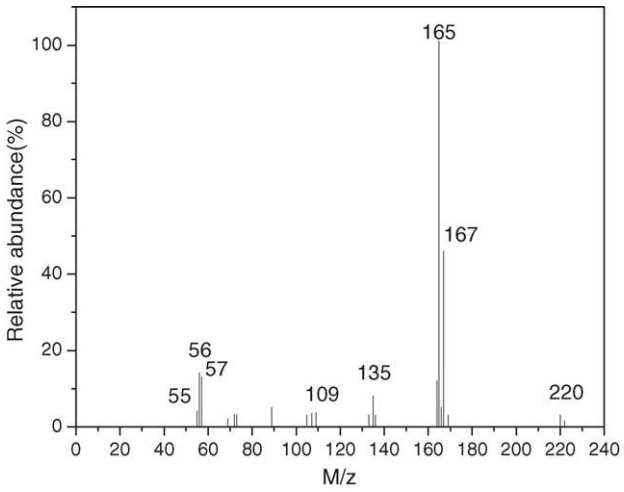

Fig. 10. Mass spectrum of compound (VIII).

3.7. Mechanism study

Irradiation of TiO_2 particles under UV light (<380 nm) that carries energy greater than the band gap (3.2 eV) induces electrons (e^-) and positive holes (h^+). These charged species can generate oxidizing species ($^\bullet OH$, H_2O_2, $HOO^\bullet$ and $O_2^{\bullet -}$) in water. The detailed mechanism of such transformation has been discussed previously in literatures [3–6] and briefly summarized here. Active species and positive holes have been recognized as the primary oxidizing agents in photocatalysis, which can in turn attack and degrade organic substrates allowing in most cases their complete mineralization.

$$TiO_2 \xrightarrow{h\nu} e^- + h^+ \quad (1)$$

$$h^+ + e^- \rightarrow N + \text{energy} \quad (2)$$

$$h^+ + H_2O_{ad} \rightarrow {}^\bullet OH_{ad} + H^+ \quad (3)$$

$$h^+ + OH^- \rightarrow {}^\bullet OH \quad (4)$$

$$e^- + O_2 \rightarrow O_2^{\bullet -} \quad (5)$$

$$O_2^- + H_2O \rightarrow HOO^\bullet + OH^- \quad (6)$$

$$2HOO^\bullet \rightarrow H_2O_2 + O_2 \quad (7)$$

$$H_2O_2 + e^- \rightarrow {}^\bullet OH + OH^- \quad (8)$$

Under natural conditions (pH 6.0), the positively charged surface of TiO_2 in pyridaben/TiO_2 system permits model molecules to be chemisorbed on TiO_2 particles by electrostatic interaction. The most negative point charge of the pyrid-

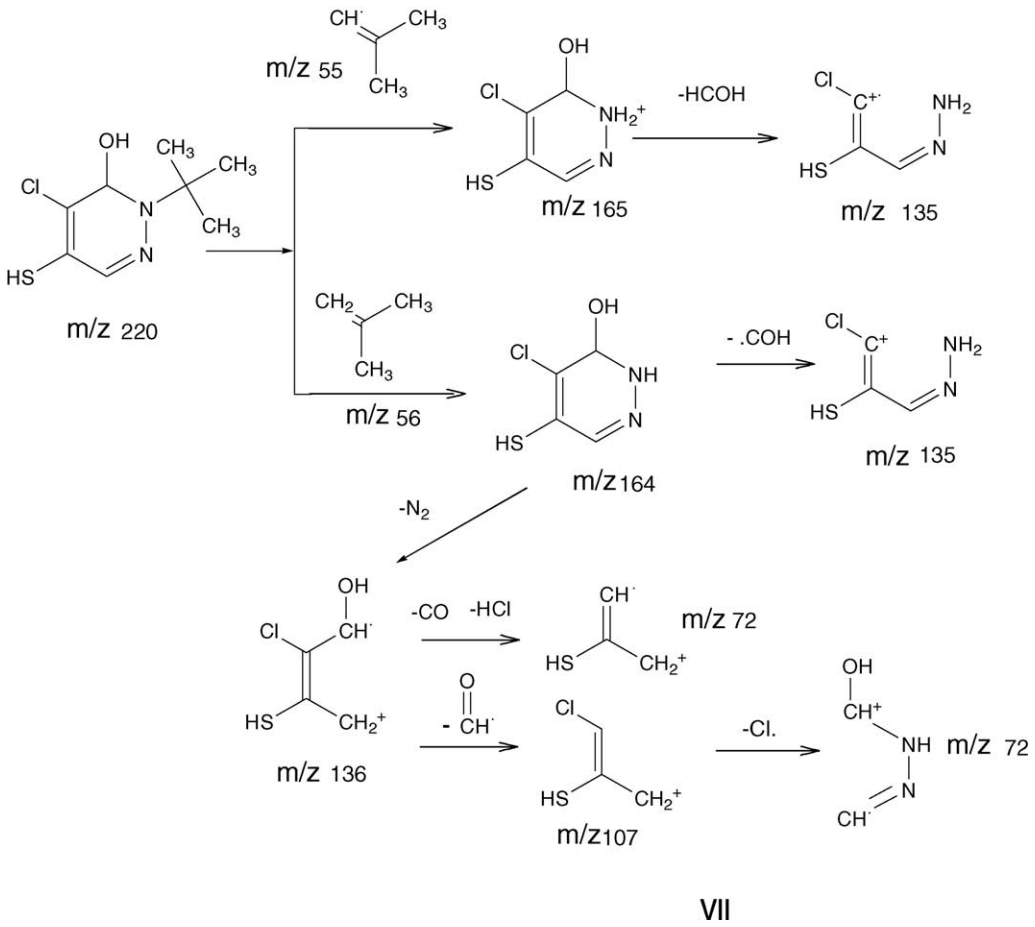

Fig. 11. MS interpretation of compound (VII).

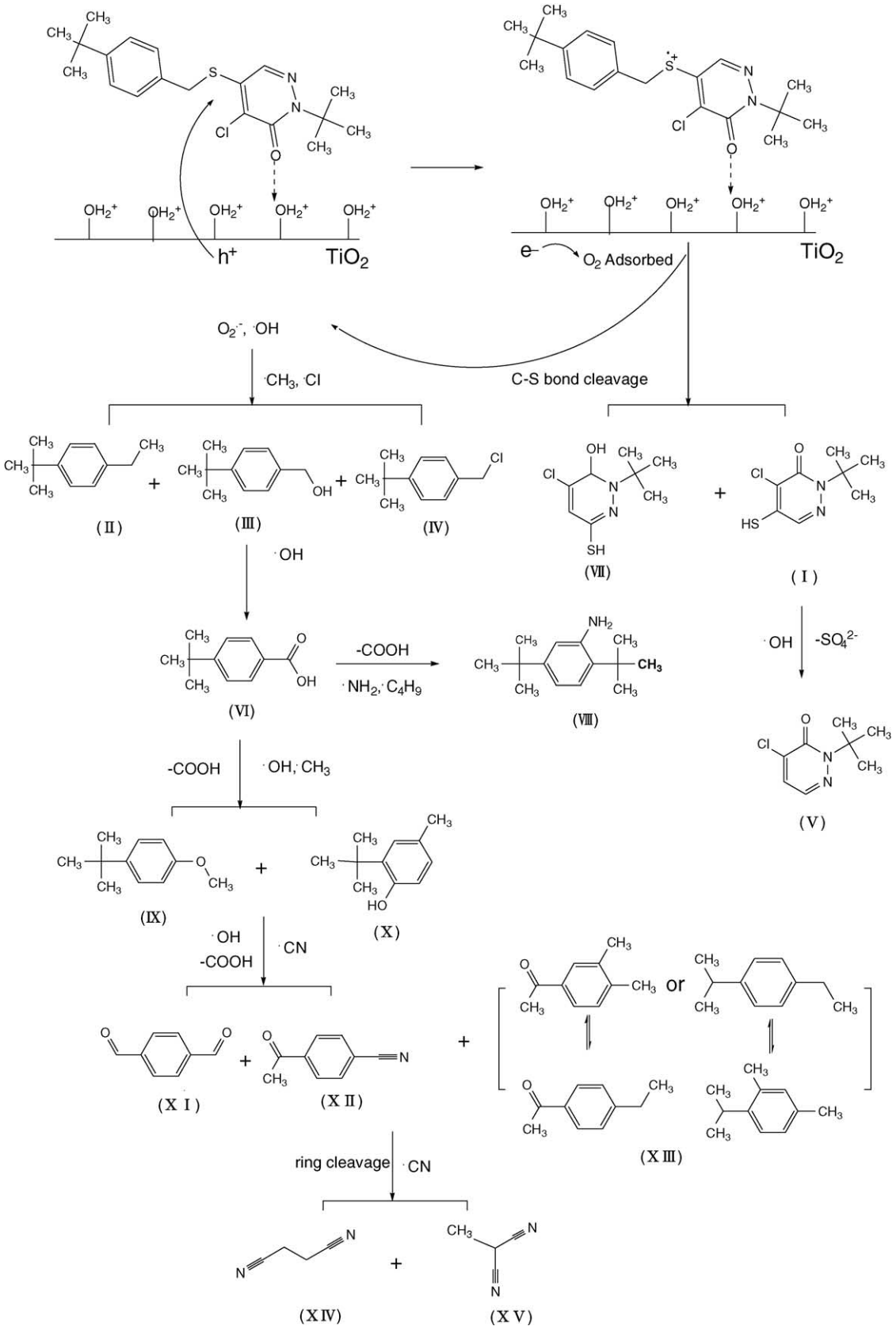

Fig. 12. Proposed photocatalytic degradation route for pyridaben.

aben structure is located at the oxygen atom O^{23} so that the adsorption involves the negative carbonyl group, which is also evidenced by the influence of pH. The point charge calculation is reported in Table 3 and the adsorption model is established in Fig. 12.

It is generally accepted that the substrate adsorption on the surface of semiconductors plays an important role in photocatalytic oxidation [3,26,27], therefore the following photocatalytic degradation process could be better rationalized by two kinds of oxidative agents: the positive holes mainly involved in the direct charge transfer of adsorbed pyridaben and the hydroxyl radicals, which are known as strongly active and degrading agents in indirect addition/substitution reaction [1,14]. Firstly, the scission of C–S functional group between phenyl ring and heterocyclic group in pyridaben molecule is considered to involve positive holes' attacking, i.e. the result of direct oxidation effect. As reported earlier [10], C–S bond should be an attacking site of pyridaben under the examined photocatalytic conditions. In this work, by calculating the length of C–S bond 1.8325 Å, as represented in Table 3, we confirm that it possesses less stability and is easier to cleave.

1-*tert*-Butyl-4-methylbenzene radicals, the fragment of C–S bond cleavage react with $^{\bullet}Cl$, $^{\bullet}CH_3$ or $^{\bullet}OH$ radicals, leading to the formation of observed products II, III and IV, respectively. $^{\bullet}Cl$ radicals are regarded as fission from heterocyclic compounds, of which the dechlorination of heterocycle is due either to the substitution of $^{\bullet}Cl$ by $^{\bullet}OH$ or the reduction by electrons of the conduction band. The formation of $^{\bullet}CH_3$ radicals may be attributed to the cleavage of solvent molecules or Photo–Kolbe reaction of short-chain acids of the ring-opened compounds, such as,

$$CH_3COOH \xrightarrow[\text{Photo-Kolbe}]{-COOH} {}^{\bullet}CH_3$$

The above intermediates could be further attacked on the aliphatic chain by $^{\bullet}OH$ radicals to form compound VI.

As previously observed, compound VI could decarboxylate via Photo–Kolbe reaction, followed by addition of $^{\bullet}C_4H_7$ and $^{\bullet}NH_2$ radicals to give compound VIII (Fig. 13). Isobutyl radicals were suggested from phenyl group or heterocycle involved positive holes' attack. Whereas, $^{\bullet}NH_2$ radicals were generated from the photodegradation of acetonitrile or from the photomineralization of heterocyclic group.

Acetonitrile is an extremely stable molecule. It is usually used as a solvent in photocatalytic oxidation reactions and is often found in industrial wastewaters. Davit et al. [28] and Lichtin and Avudaithai [29] reported the feasibility of the photocatalytic oxidation of acetonitrile in liquid phase. They found that CH_3CN could occur hemolytic dissociation of the C–C bond to generate $^{\bullet}CH_3$ and $^{\bullet}CN$ radicals, which suggested that the interaction of holes and electrons cause the dissociation of CH_3CN. Furthermore, Zhuang et al. [30] studied TiO_2 photooxidation acetonitrile and indicated that the final oxidation products were CO_2 and H_2O, and ammonia was also checked as one of the photoreaction products [28]. Therefore, the total degradation chart of $^{\bullet}CN$ radicals could be understood briefly as following:

$$^{\bullet}CN + e^- \rightarrow CN^-$$

$$CN^- \xrightarrow{TiO_2,hv} CNO^- \xrightarrow{TiO_2,hv} NH_2OH + HCO_3^-/CO_3^{2-}$$

$$\xrightarrow{TiO_2,hv} NH_3 + N_2 + NO + N_2O + H_2O + CO_2$$

In our experiments, the presence of compounds X, IV, XV and XII is further confirmed the formation of $^{\bullet}CN$ radicals.

$^{\bullet}OH$ and $^{\bullet}CH_3$ radicals are primary responsible for the successive oxidation elimination, substitution and decarboxylation processes, leading to a series of compounds IX, X, XI and XIII.

Aliphatic intermediates XIV and XV were proposed by opening of the aromatic ring or heterocycle, followed by substitution of $^{\bullet}CN$ radicals from CH_3CN solution. The above consideration leads us to postulate the reaction mechanism for the photocatalytic degradation of pesticide pyridaben by $\lambda \geq 360$ nm irradiation, shown in Fig. 12.

Based on the GC–MS spectra obtained from pyridaben solutions collected at different time intervals, a semiquantitative evaluation of the mainly aromatic compounds during the course of the experiment was carried out by expressing the areas of the corresponding GC peak as functions of irradiation time. The evolutions of pyridaben and most of intermediates are depicted up to 450 min in Figs. 14–17, respectively. By describing the typical bell-shaped profiles in most of the cases, we clearly observed the change in the distribution of each intermediate during the photocatalytic degradation of pyridaben. It is indicated that during the first 200 min of the photoreaction, several compounds including I, II, II, IV and VII appear in maximum amount. These compounds may be considered as degradation products in the first step, originating from oxidative cleavage of the C–S bond of the substrate molecule.

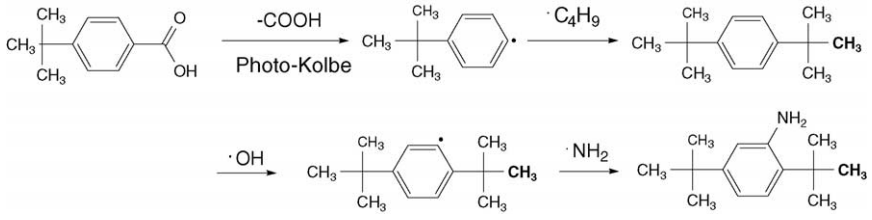

Fig. 13. Proposed reaction scheme for the formation of transformation product VIII.

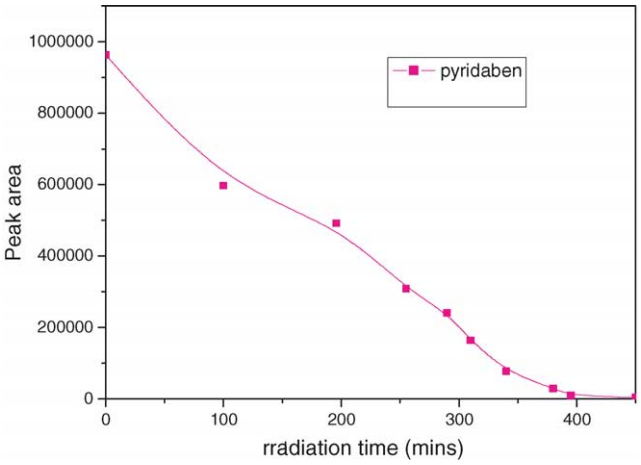

Fig. 14. Disappearance of pyridanben.

According to the data of Fig. 15, compounds I, III and IV were formed, reaching their maximum concentration at 200 min and then disappeared, when the abatement of pyridaben is about 50%. Compound VI was present at lower concentrations, but it was considered as main intermediates, because it was abundantly detected at 310 min irradiation. The successive appearance of the maximal quantity of above two kinds of intermediates indicates the dealkylation paths by oxidation side chains adjacent to the phenyl ring to be a stepwise process.

Fig. 16 shows a comparison between the kinetic curves of heterocyclic compounds. Smaller amount intermediates such as I and VII appear almost together with the early phenyl pieces, while V appears with a delay. By comparing these curves, it seems that the desulfonylation via the pyridazine ring is more efficient and confirms the conversion for compound I to compound V. The photocatalytic kinetics of intermediate VII is nearly as same as compound I, but it forms by a larger extent. The conditions of the analysis did not allow for the detection of small-ring fragment compounds.

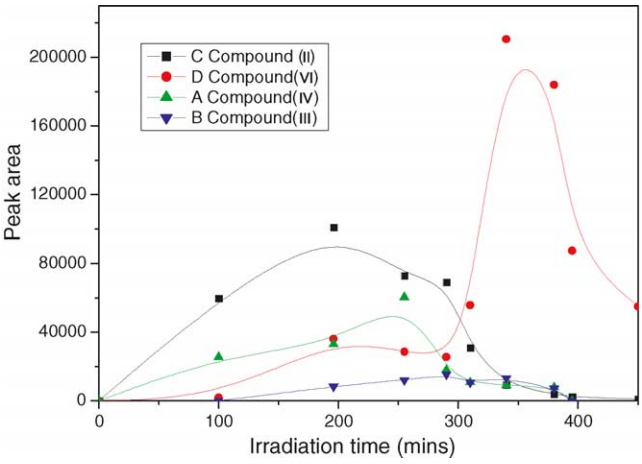

Fig. 15. Evolution of photoproducts II, III, IV and VI during pyridaben photocatalytic degradation.

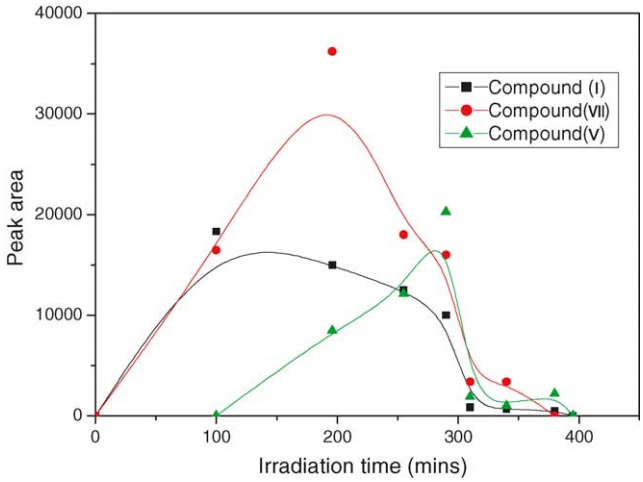

Fig. 16. Evolution of photoproducts I, IV and VII during pyridaben photocatalytic degradation.

Fig. 17 suggests compound VI be further oxidized to form dealkylation compounds. After irradiation of 310 min, compounds XI and XIII, the intermediates before phenyl ring cleavage, were detected at appreciable concentrations. Compound XIII corresponds to further attacked on the isobutanyl chain by •OH radicals, and then decarboxylates into CO_2 via Photo–Kolbe reaction, attaining a maximum concentration at 400 min. Fragment VIII appears already in small quantities at the beginning of the reaction. Its concentration increases with time of irradiation and goes through maximum at 380 min.

Another question of interest is the detection of the critical oxidative steps throughout the process. Compounds II and VI may be considered as the main process DPs, as shown in Fig. 15, due to their high concentration compared with other main intermediates detected, but they also disappear gradually. The results imply that these compounds be not resistant to degradation during photocatalysis.

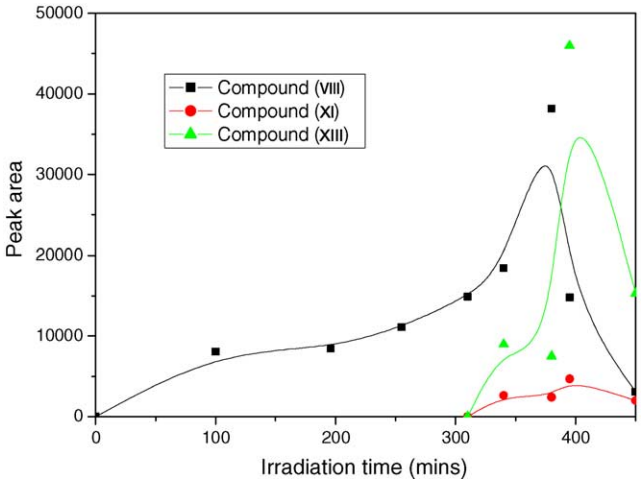

Fig. 17. Formation of intermediates VIII, XI and XIII during pyridaben photocatalytic degradation.

The great number of compounds during the degradation of pyridaben shows the complexity of the photocatalytic process. Based on the results of the present study, mechanistic information can be extracted with respect to the steps involved in the photoreaction, from adsorption of the substrate on the photocatalyst surface to the formation of intermediates and final products in the solution. It can also be concluded that none of the DPs formed limits the reaction kinetics.

4. Conclusions

The photocatalytic degradation of pyridaben solutions has been examined with the use of UV-irradiated TiO_2 catalyst. The direct photolysis and heterogeneous photocatalysis were studied by shorter ($\lambda \geq 300$ nm) and longer wavelength ($\lambda \geq 360$ nm) irradiation. Photocatalytic degradation of pyridaben was more dominant at $\lambda \geq 360$ nm than at $\lambda \geq 300$ nm irradiation, in other words, the use of TiO_2 for photocatalysis at UV ≥ 300 nm is not an effective process. Therefore, it is important to properly choose the irradiation wavelength in photocatalytic degradation.

On kinetic study, the effect of the dose of the semiconductor in the photocatalytic reaction has suggested that the degradation rate of pyridaben increase with the dosages of TiO_2, while an overdose of catalyst would retard the reaction. In addition, solvent effect, pH effect and radiant flux were also examined, with results indicating that the degradation kinetics is strongly dependent on these factors.

A detailed reaction mechanism was presented from the initial step of adsorption pyridaben molecule on the photocatalyst surface to interaction with active species generated by irradiating TiO_2, and then the substrate molecule cleaved to benzene and heterocyclic fractions; finally, the primary reaction intermediates underwent a series of oxidation steps leading to the formation of short-chain compounds. The kinetics of the formation and decomposition of some of the degradation intermediates were semiquantified by GC–MS. Typically bell-shaped profiles of their kinetic behavior clearly confirmed that the aromatic compounds could be progressively degraded to lower molecular weight through a series of oxidation steps.

Acknowledgement

This work is financially supported by Hi-Tech Research and Development Program (863 Program) of China (No. 2002AA302304). We would like to thank the National Natural Science Foundation of China.

References

[1] M. Pera-Titus, V. Garcĭıa-Molina, M. Baños, J. Giménez, S. Esplugas, Appl. Catal. B 47 (2004) 219.
[2] D. Ollis, Environ. Sci. Technol. 19 (1985) 480.
[3] J. Herrmann, Catal. Today 53 (1999) 115.
[4] A. Mills, S. Hunte, J. Photochem. Photobiol. A 108 (1997) 1.
[5] A. Fujishima, T. Rao, D. Tryk, J. Photochem. Photobiol. C 1 (2000) 1.
[6] M.A. Fox, M.T. Dulay, Chem. Rev. 93 (1993) 341.
[7] P. Cabras, A. Angiono, V.L. Garau, M. Melis, F.M. Pirisi, F. Cabitza, F. Dedoia, S. Navickiene, J. Agric. Food. Chem. 46 (1998) 4255.
[8] O. Hajime, S. Aakamoto, J. Pesticide Sci. 19 (1994) 243.
[9] A. Valverde, A. Aguilera, M. Rodriaguez, M. Boulaid, M. Soussi-El Begrani, J. Agric. Food. Chem. 50 (2002) 7303.
[10] X. Zhu, X. Feng, C. Yuan, X. Cao, J. Li, J. Mol. Catal. A 214 (2004) 293.
[11] C. Hu, Y. Wang, H. Tang, Chemosphere 41 (2000) 1205.
[12] C. Wong, W. Chu, Chemosphere 50 (2003) 981.
[13] A. Assabane, Y. Ichou, H. Tahiri, C. Guillard, J. Herrmann, Appl. Catal. B 24 (2000) 71.
[14] A. Houas, H. Lachheb, M. Ksibi, E. Elaloui, C. Guillard, J. Herrmann, Appl. Catal. B 31 (2001) 145.
[15] S. Horikoshi, A. Saitou, H. Hidaka, Environ. Sci. Technol. 37 (2003) 5813.
[16] C. Guillard, S. Horikoshi, N. Watanabe, H. Hidaka, P. Pichat, J. Photochem. Photobiol. A 149 (2002) 155.
[17] S. Horikoshi, N. Serpone, S. Yoshizawa, J. Knowland, H. Hidaka, J. Photochem. Photobiol. A 120 (1999) 63.
[18] S. Horikoshi, N. Serpone, J. Zhao, H. Hidak, J. Photochem. Photobiol. A 118 (1998) 123.
[19] P. Fernandez-Ibanez, F. Nieves, S. Malato, J. Colloid Interface Sci. 227 (2000) 510.
[20] A. Piscopo, D. Robert, J. Weber, Appl. Catal. B 35 (2001) 117.
[21] S. Parra, S. Stanca, I. Guasaquillo, K. Thampi, Appl. Catal. B 51 (2004) 107.
[22] M. Sokmen, D. Allen, A. Hewson, M. Clench, J. Photochem. Photobiol. A 141 (2001) 63.
[23] L. Moeini-Nombel, S. Matsuzawa, J. Photochem. Photobiol. A 119 (1998) 15.
[24] S. Matsuzawa, J. Tanaka, S. Sato, T. Ibusuki, J. Photochem. Photobiol. A 149 (2002) 183.
[25] J. D'Oiivelra, G. Ai-Sayyed, P. Pichat, Environ. Sci. Technol. 24 (1990) 990.
[26] M. Stylidi, D. Kondarides, X. Verykios, Appl. Catal. B 47 (2004) 189.
[27] M. Stylidi, D. Kondarides, X. Verykios, Appl. Catal. B 40 (2003) 271.
[28] P. Davit, G. Martra, S. Coluccia, V. Augugliaro, E. Garc'ıa López, V. Loddob, G. Marc'ı, L. Palmisano, M. Schiavello, J. Mol. Catal. A 204–205 (2003) 693.
[29] N. Lichtin, M. Avudaithai, Environ. Sci. Technol. 30 (1996) 2014.
[30] J. Zhuang, C. Rusu, J. Yates, J. Phys. Chem. B 103 (1999) 6957.